Electronic properties and redox chemistry of N-confused metalloporphyrins

Frederico F. Martins,[a] Marcel Swart[a,b*]

[a] *IQCC & Dept. Química, Universitat de Girona, Campus Montilivi (Ciències), 17003 Girona, Spain*
[b] *ICREA, Pg. Lluís Companys 23, 08010 Barcelona, Spain*

Received date (to be automatically inserted after your manuscript is submitted)

Accepted date (to be automatically inserted after your manuscript is accepted)

ABSTRACT: Here we study the effect of metals on the characteristic Soret band of N-confused porphyrins. We used DFT calculations to study how this low-lying region of the spectrum of the NCP-2H isomer is affected by the introduction of transition metals with various (d^2, d^3, d^4 and d^5) d-electron configurations. The spin ground state of these complexes is mostly dependent on the number of unpaired electrons, both with and without the presence of an axial ligand. The analysis of the electronic distribution and spin density showed that these unpaired electrons are often harbored by the N-confused porphyrin ring instead of on the metal. Time-dependent DFT results indicated that the aromatic system of porphyrin is disrupted in the N-confused isomer: instead of the typical large Soret band, this now gives rise to two peaks of much lower intensity. Most metallo-porphyrins exhibited similar optical properties, with the HOMO/LUMO orbitals showing a mixed metal/porphyrin character. The only exception was the Rh metalloporphyrin that exhibited a ligand-to-metal charge transfer band with increasing intensity as function of the ligand field. This suggests Rh is the only metal whose orbitals are higher in energy than the ligand's, indicating that it is the only system where the redox processes occur on the metal.

KEYWORDS: Metalloporphyrins, N-confused porphyrins, Electronic configuration, DFT, Ligand effects.

*Correspondence to: Marcel Swart, Univ. Girona, marcel.swart@gmail.com.

INTRODUCTION

Porphyrin-like motives found in biological molecules such as the heme group[1], vitamin B12[2] or chlorophylls[3] inspired chemists to synthesize tetraphenylporphyrin (TPP), octaethyl porphyrin (OEP), and many other derivatives, transition-metal complexes and materials with all kinds of interesting properties.[4] Eventually, studies turned to its isomers and new porphyrinoids have been created.[5] The first N-confused porphyrin (NCP) (see Scheme 1) was synthesized in 1994.[6,7] Two of its tautomers were later successfully isolated depending on the solvent: NCP-3H and NCP-2H,[8] which, in conjunction with DFT[9] calculations, allowed for the study of their individual properties,[10-12] unraveling their promise for application such as the development of new photodynamic therapeutics.[13] NCP-3H exhibited a higher degree of aromaticity and was thus considered to be more stable. Nevertheless, transition-metal complexes with both tautomers have been synthesized[14-17] and they are often interconvertible via redox reactions. The possibility of forming neutral molecules when combined with M^{II} and M^{IV} (with axial ligands) metal ions with decreased steric hindrance at its center, or of the derivatization of the outer N-H bond, however, confer additional interest to the NCP-2H form.

The complexes of such ligands have become a hot topic due to their prospective anti-cancer activity,[18] CO_2 fixation/derivatization capabilities[19-21] and ability to function as molecular (anion) sensors[22] or photosensitizers.[23] The properties of these compounds have been tentatively rationalized with analyses of the relative energy differences of their frontier orbitals (ΔHOMO and ΔLUMO)[24] which are mainly located at the porphyrin ring and barely mixed with the metal *d* orbitals. However, these compounds have been obtained in the bare porphyrin forms, with axial ligands[25] and even as metal-metal bonded dimers,[26] and there is no explanation for this preference or its consequences on the properties of these compounds. The repercussions of changing the metal center have also not been explored, especially with regards to spin state which is often not reported.

Here, we study a series of Cr(II), Cr(III), Mo(II), Mo(IV), Os(II), Os(IV), Rh(III) complexes with the N-confused porphyrin NCP-2H to understand the different forms in which they are obtained, focusing on their spin state and electronic structure.

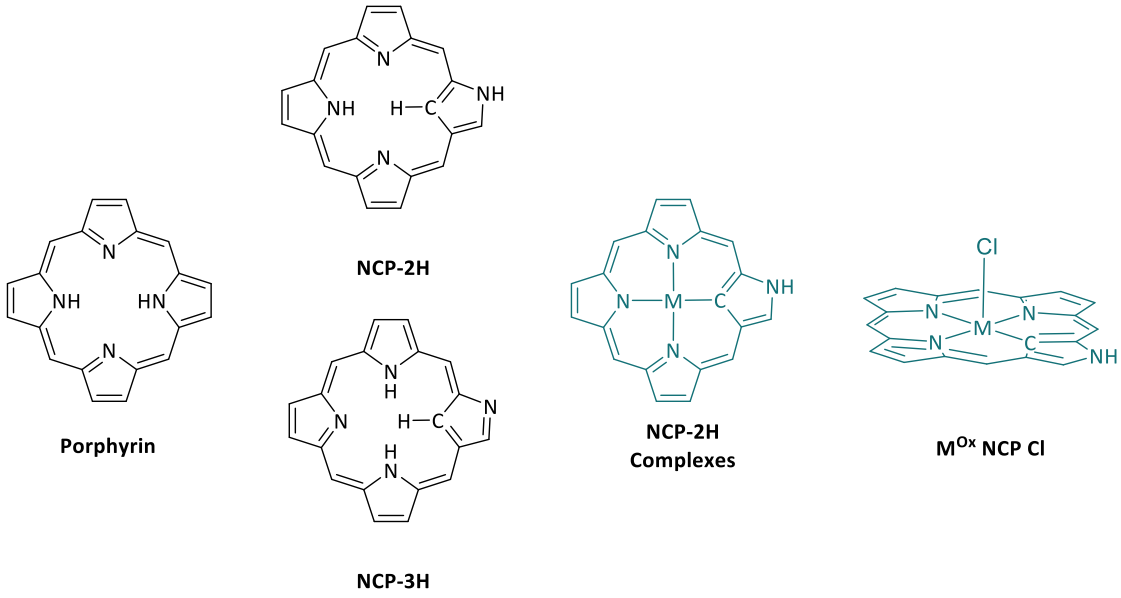

Scheme 1. Schematic structure of a porphyrin, its N-confused isomers including the one used as a ligand here, and corresponding transition-metal complexes. The latter two are analyzed in the present work: M = $Cr^{II/III}$, $Mo^{II/IV}$, $Os^{II/IV}$, Rh^{III}.

METHOD VALIDATION

To the best of our knowledge, no X-ray structures are available in the CCDC database for N-confused porphyrins. Luckily, previous results had indicated that the methodology developed in-house for determining bond-orders[27] based on the S12g functional[28] was successful in the description of the properties of porphyrin transition metal complexes. However, because of the diversity of coordination environments of the metal in (confused) porphyrins with different axial ligands, we started by testing our computational method against experimental data available in the literature for porphyrin-chloride systems.

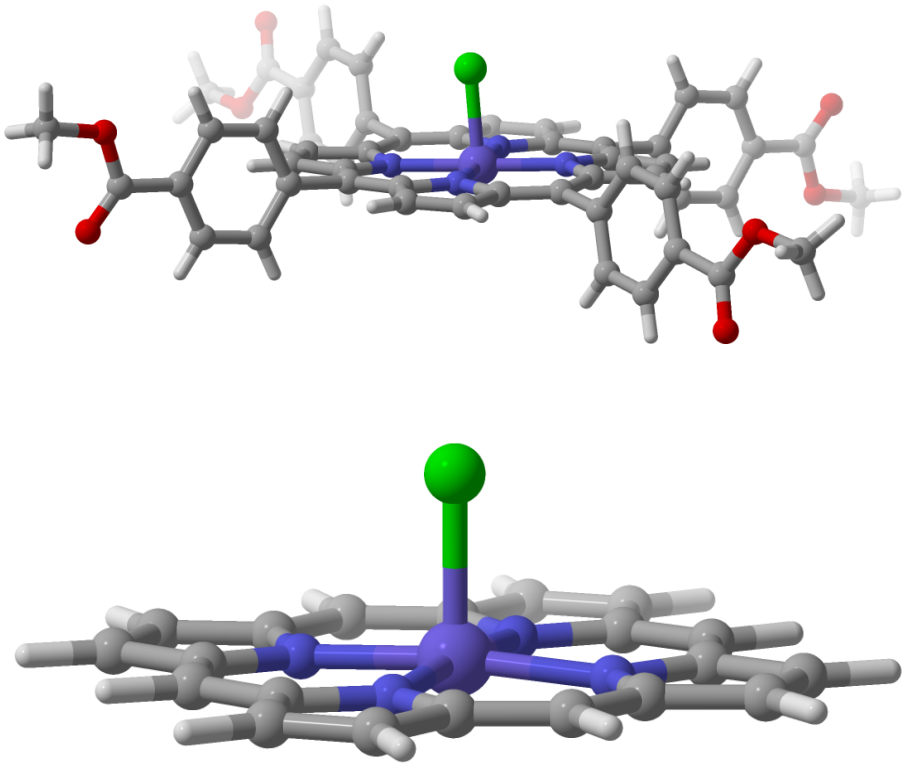

Fig. 1. Example of the X-ray crystal structure of the Rh(porph)Cl complex reported in the literature (top, CCDC code JETBUI[29]), and our computational model (bottom).

Metal-Cl porphyrin structures were retrieved from the Cambridge Crystallographic Data Center database with Cr, Rh and Os, reorganized and simplified to a model which was devoid of substituents on the porphyrin ring (Figure 1). The models were then optimized with S12g/TZ2P (including solvent and relativistic effects, see Computational details) in all the relevant spin states and their energy minima were analyzed. Comparison of these results to those available in the original literature reports can be found in Table 1.

Table 1. Comparison between M-Cl distance and ground spin state of the complexes reported in the literature and our computational models

	M-Cl (Å)		Ground state (S)		CCDC	ref
	Exp.	DFT	Exp.	DFT		
$Cr^{III}(Cl)(H_2O)$	2.321	2.296	3/2	3/2	ROTKES	[30]
$Os^{IV}(Cl)_2$	2.293	2.324	1[a)]	1	ZAVLIR	[31]
$Rh^{III}Cl$	2.204	2.261	0	0	JETBUI	[29]

a) Actual magnetic moment measured was slightly lower than expected for S=1.

The coordination environment in our computational models is the same as that found in the crystal structure: a Cl axial ligand was added in the case of Rh, two in the case of Os and one Cl and one water molecule in the case of Cr. Indeed, our models proved to be good representations of the full complexes that had been synthesized, thus showing the minor effect of the porphyrin substituents on the structural and electronic properties of the metal center. The correct ground (spin) state was

predicted for all three complexes using the chosen method, S12g/TZ2P. The largest M-Cl bond distance differences between theory and experiment were obtained for the Os^{IV} complex (0.031 Å, 1.4%) and the Rh^{III} (0.057 Å, 2.6%) meaning that the DFT geometries are also in good agreement with the single crystal X-ray results. Further details on the geometrical properties and relative energies of these complexes can be found in Tables S1-S3.

RESULTS AND DISCUSSION

We have confirmed the reliability of the S12g functional for the systems at hand (see Method validation) and are now able to delve deeper into the electronic properties of these N-confused metalloporphyrins. A correct spin ground state is crucial for the shape and electronic transitions of these molecules; hence it must be analyzed first. This was performed not only for the bare metallo-N-confused porphyrin, but also for the analogues with a negatively charged axial ligand from each end of the spectrochemical series (Cl^- and CN^-). We chose monoanions to keep the total charge of the final complexes at the bare minimum. The results are presented consecutively, with increasing number of *d* electrons, from d^2 in the Mo(IV) NCPs to d^6 in the case of those bearing Os(II) or Rh(III) metal ions.

Spin state

d^2 and d^3 populations

The two cations with the lowest *d*-electron count are $Mo^{IV}(4d^2)$ and $Cr^{III}(3d^3)$. Energies of the possible spin states, relative to the lowest lying state, for their NCP complexes are represented in Scheme 2.

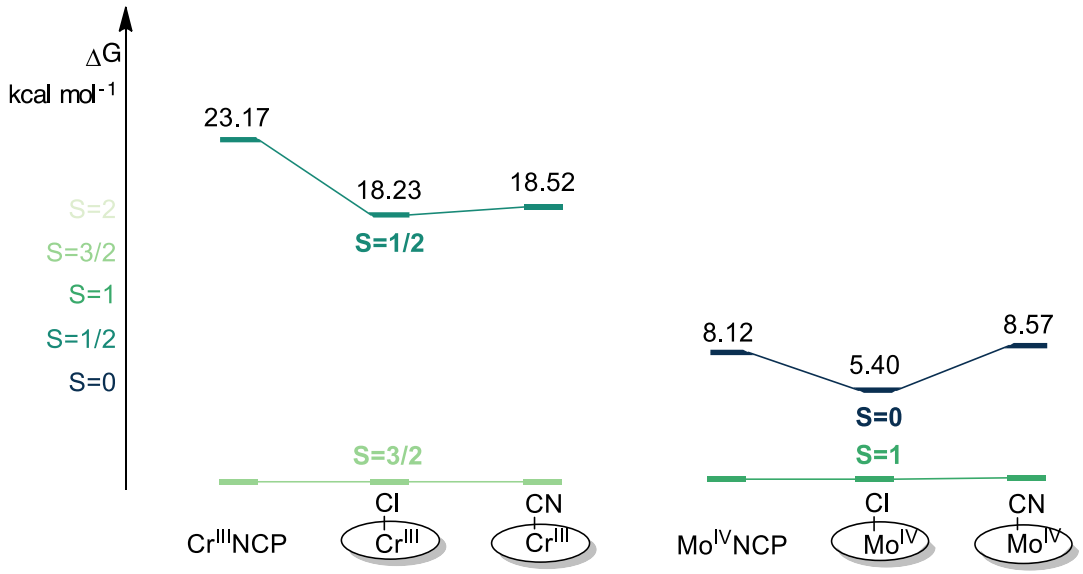

Scheme 2. Spin state relative energies for Cr^{III} and Mo^{IV} N-confused porphyrins and their pentacoordinate analogues.

In both cases, a high-spin (S=3/2 and S=1, for chromium and molybdenum, respectively) electronic distribution is shown to be more stable for the bare N-confused porphyrins. The same effect is observed upon addition of the axial ligands for the d^2 and d^3 populations: the low-spin state is slightly

stabilized by the low-field inducing chloride anion, but this stabilization is counteracted by the high-field axial ligand cyanide. Nevertheless, no spin state change is to be expected when moving from the square planar to square pyramidal coordination sphere.

d^4 population

Three metal ions studied here have a d^4 population: Cr^{II} ($3d^4$), Mo^{II} ($4d^4$) and Ov^{IV} ($5d^4$). This series provides insight into the effect of core potential as each metal belongs to a different period of the periodic table. Results are in Scheme 3.

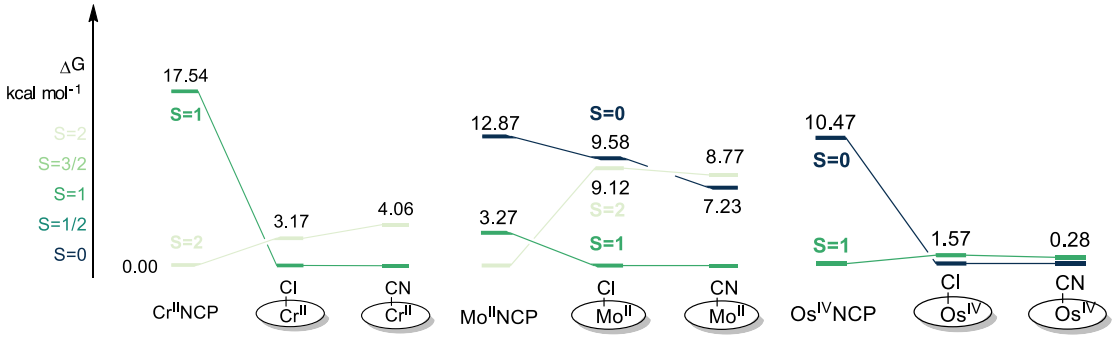

Scheme 3. Spin state relative energies for Md^4 N-confused porphyrins and their pentacoordinate analogues.

The core potential is not affecting the spin state, as similar energy profiles were obtained for the three metal centers. A high-spin state is the most favorable for the bare metal NCPs (S=2 for Cr^{II} and Mo^{II}, S=1 for Os^{IV}), but the coordination of an axial ligand, even with a low field strength, stabilizes a lower spin configuration to such extent that a spin change is to be expected. In the case of osmium, energy differences close to the chemical accuracy limit (1.57 kcal mol^{-1} and 0.28 kcal mol^{-1}) are obtained, so it is possible that a mixed spin distribution is measured experimentally, depending on the temperature. However, the increase in Δ_{SP} to a point that it matches or is greater than the spin pairing energy and the qualitative similarity to the other two energy profiles are clear.

d^5 population

The metal ions with the highest *d* electron population are Rh^{III}($4d^5$) and Os^{II}($5d^5$). The results obtained for those metalloporphyrin complexes are in Scheme 4. Energies above 33 kcal mol^{-1} are not represented to scale.

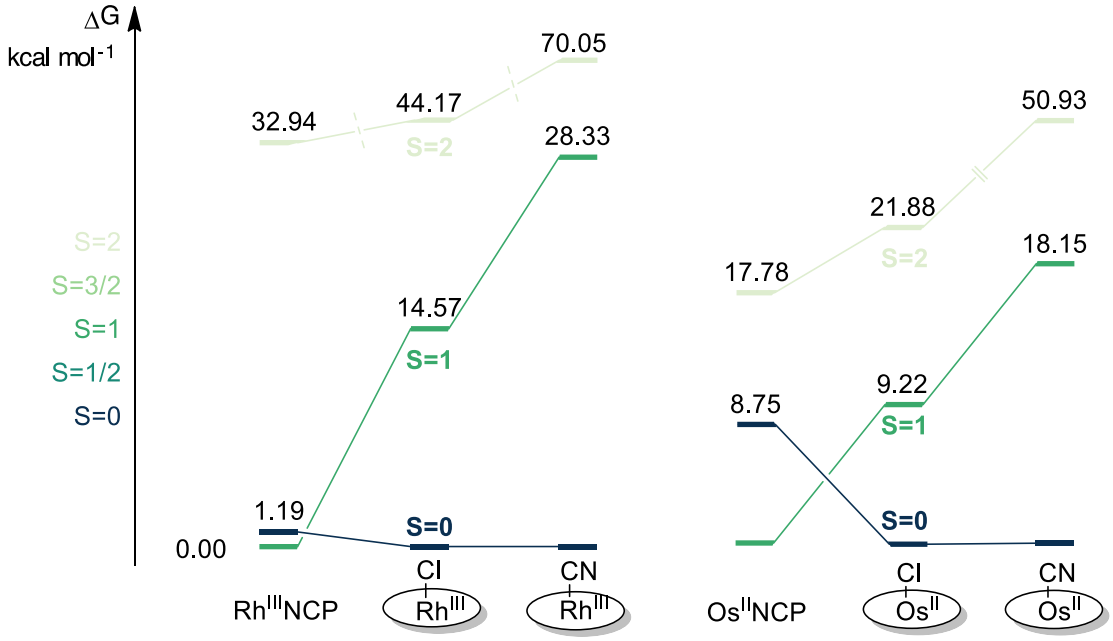

Scheme 4. Spin state relative energies for Md^5 N-confused porphyrins and their pentacoordinate analogues.

We have again obtained comparable energy profiles for the two metals. The S=2 high-spin configuration is too high in energy for the bare NCP complexes and those with an axial ligand, regardless of the metal center. The intermediate spin state is the most stable for the square planar complexes, but the low-spin (S=0) configuration is clearly the most stable for the complexes with axial ligands.

A summary of the results presented above can be found in Table 2.

Table 2. Summary of the results presented above on the spin state of the complexes.

	Ground state (S)				
	d^2	d^3	d^4		d^5
M(NCP)	1	3/2	2	1	1
M(NCP)Cl	1	3/2	1	0	0
M(NCP)CN	1	3/2	1	0	0

The same spin states and energy profiles were obtained for the complexes with equal *d* electron count; they seem to depend only on the number of *d* electrons on not on the charge of the metal or even the total charge of the complexes. The exception to this rule was Os^{IV} which, despite having a similar energy profile to the remaining d^4 complexes, can stabilize lower spin states even further. The coordination to an additional axial ligand can either have no effect on the spin state, for smaller *d* orbital populations, or allow for the stabilization of a lower spin configuration via increase of the energy difference between the stabilized and the destabilized *d* orbitals. This, however, is occurring simply due to the destabilization of the d_{z^2} orbital upon axial ligand coordination: the strong field ligand cyanide would generally only extend the effect of the low field chloride, further destabilizing already higher energy electronic configurations.

As shown before, the present computational method proved to be accurate in assigning the spin state of metallo porphyrinate complexes. Porphyrin derivatives, however, are known non-innocent

ligands[32] so a careful look into the electronic structure of these complexes must be carried out to understand if all of the spin density in these complexes is located in the metal centers or if the NCP ring is the entity that will participate in redox processes involving these complexes. This may occur even if the aromatic system is disrupted by the N-confusion. The combination of a population analysis of molecular orbitals with great *d*-character with the mapping of the Mulliken spin densities should provide this information.

For both d^5 metallo-N-confused porphyrins, a S=1ground spin state was obtained. This would correspond to a low-spin state in the square-planar ligand field, with two filled *d*-based molecular orbitals (4 electrons) and two SOMOs. A Sit analysis[33] of the *d*-orbital occupations reveals a total of four electrons. This means that instead of the expected Rh(III) and Os(II) cations, we formally observe the coupling of Rh(IV) and Os(IV) with ligand radicals, $Rh^{IV}NCP^{\bullet}$ and $Os^{IV}NCP^{\bullet\bullet}$. From a ligand-field point of view, this can be rationalized as the low-lying *d*-orbitals will all be partially occupied, thus increasing the stability of the complexes. The spin-density, however, is in different parts of the NCP ring (Scheme 5). In the case of the Rh NCP, there is one highly localized unpaired electron on the confused carbon atom and the remaining electron is delocalized over the four N-confused porphyrin C_β. In the case of the Os NCP, the two electrons are completely delocalized over the outer ring of the ligand.

The Os(IV) NCP complex is correctly described as bearing formal Os(IV). This agrees with the above observation: Osmium will always prefer to have four unpaired *d* electrons and redox processes are expected to occur on the ligand. A similar observation is made for the molybdenum metal ions: the Mo(II) complex is best described as formal Mo(IV) coupled with a Mo(II) diradical as similar spin densities are obtained for the metal center and only two SOMOs were obtained. Finally, the same was observed for the theoretical Cr(II) NCP, which instead is better described as $Cr^{III}NCP^{\bullet}$ indicating that reduction of the Cr(III) compound would reduce the ligand and not the metal.

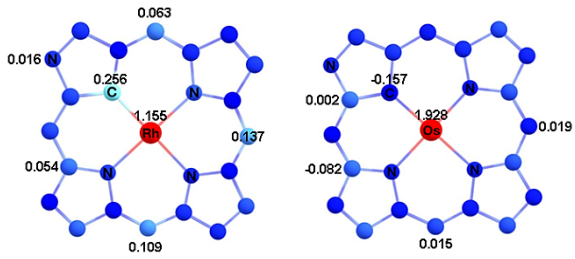

Scheme 5. Mulliken spin density atom coloring from dark blue (˜0.0) to red (> 1.0) for the lowest spin states of Rh(NCP) and Os^{II}(NCP) – the latter is representative of the remaining M(NCP) complexes. Numbers represent the Multipole Derived Charge Analysis (q) spin densities for relevant atoms.

These preliminary results have directed us to properly investigate the electronic structure of all these compounds. We have done so via a combined oxidation state and spin density analysis (see Supporting Information Tables S4-S5). Both approaches are based on defining how many electrons are localized, in this case, at the metal and how many electrons are delocalized over the whole structure. The oxidation states can be calculated directly[34,35] from the localization and delocalization indexes as obtained from a QTAIM topology analysis.[36] As for the spin densities, these are relatively pitted against each other (metal vs porphyrin atoms) for complexes with unpaired electrons. The example for Mo^{II} complexes can be found in Scheme 6.

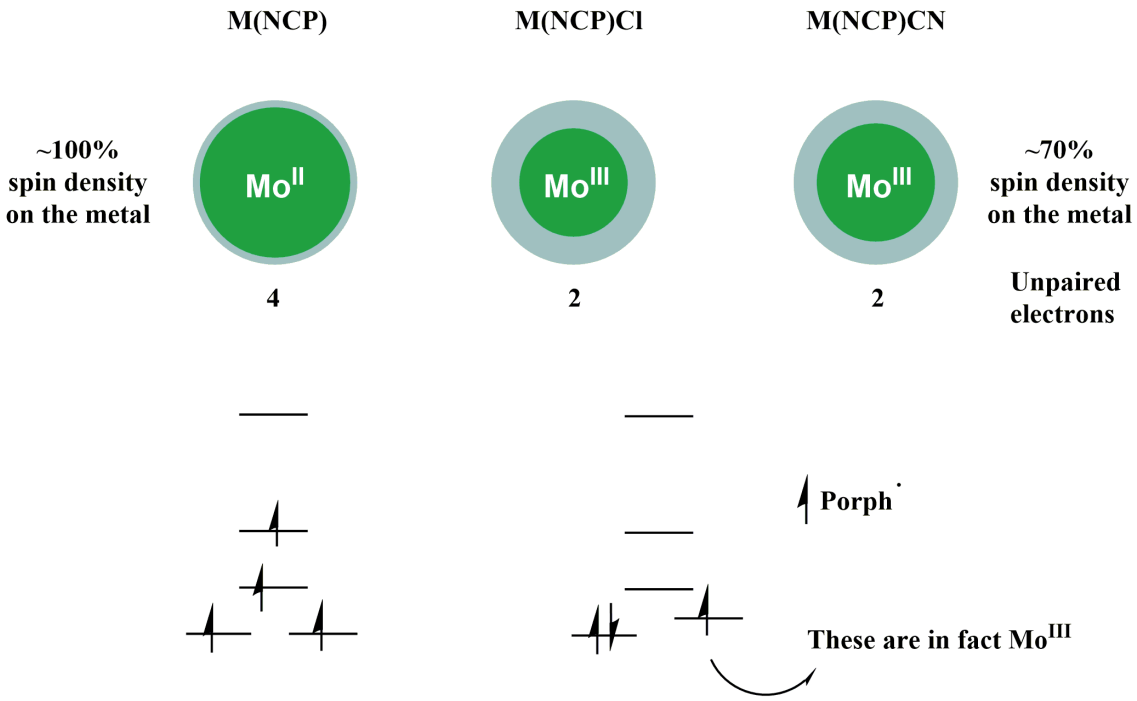

Scheme 6. Example for the theoretical Mo^{II} complexes of how the spin density localization can provide information on the electronic structure of the complexes.

A summary of the results can be found in Table 3. They show that only a limited number of oxidation states is available for most metals (Cr^{III}, Mo^{IV}, Os^{IV}) as the NCP ligand is very likely to be reduced, except for the case of rhodium in which two oxidation states can arise, $Rh^{III/IV}$.

Table 3. Electronic configuration of the metalloporphyrins.

	Formal electronic configuration (FEC)		
	M(NCP)	**M(NCP)Cl**	**M(NCP)CN**
Cr^{III}	$[Cr^{III}NCP]^{+}$	$[Cr^{III}(NCP)Cl]$	$[Cr^{III}(NCP)CN]$
Mo^{IV}	$[Mo^{IV}NCP]^{2+}$	$[Mo^{IV}(NCP)Cl]^{+}$	$[Mo^{IV}(NCP)CN]^{+}$
Cr^{II}	$[Cr^{III}(NCP^{\cdot})]$	$[Cr^{III}(NCP^{\cdot})Cl]^{-}$	$[Cr^{III}(NCP^{\cdot})CN]^{-}$
Mo^{II}	$[Mo^{IV}(NCP^{\cdot\cdot})]$	$[Mo^{IV}(NCP^{\cdot\cdot})Cl]^{-}$	$[Mo^{IV}(NCP^{\cdot\cdot})CN]^{-}$
Os^{IV}	$[Os^{IV}(NCP)]^{2+}$	$[Os^{IV}(NCP)Cl]^{+}$	$[Os^{IV}(NCP)CN]^{+}$
Os^{II}	$[Os^{IV}(NCP^{\cdot\cdot})]$	$[Os^{IV}\ (NCP^{\cdot\cdot})Cl]^{-}$	$[Os^{IV}(NCP^{\cdot\cdot})CN]^{-}$
Rh^{III}	$[Rh^{IV}(NCP^{\cdot})]^{+}$	$[Rh^{III}(NCP)Cl]$	$[Rh^{III}(NCP)CN]$

This assignation is not clear for the Rh(NCP). Therefore, we used energy decomposition analysis (EDA)[37] to further investigate the correct electronic structure in Rh(NCP) as it is not entirely clear from the spin density and localization indexes. The orbital interactions are in the table below:

Table 4. Orbital interaction energy as calculated per EDA.

	Orbital interaction stabilization (kcal mol^{-1})
$[Cr^{III}(NCP^{\cdot})]$	-813.83
$[Cr^{II}(NCP)]$	-432.73
$[Rh^{IV}(NCP^{\cdot})]^{+}$	-1488.07

$[Rh^{III}(NCP)]^{+}$	-935.67

EDA provided the expected result for chromium in which it shows that the $Cr^{III}(NCP^{\cdot})$ is the species with the greatest orbital stabilization. The same was observed for the Rh^{IV} species bound to a NCP radical instead of Rh^{III} analogue, confirming the assignation in Table 3.

We also attempted to study any correlation of these findings with the geometry of the NCP rings and their delocalized π system. The shape of porphyrins has been recently reviewed by Kingsbury and Senge.[38] Although they derive some intricate geometrical parameters, we have preferred to perform a continuous shape measurement (CShM) with SHAPE.[39,40] This measurement quantifies the difference between a selected geometry, in our case the metalloNCPs, and the geometries of ideal transition-metal complexes. We compared the bare NCP complexes to the four vertices[41] polyhedral model and the axial substituted NCPs to the five vertices[42] polyhedral. Greater distortions are expected for the latter, as axial coordination on one end only seems to be capable of pulling the metal out of plane. The results can be found in SI Table S6. The greatest distortions can be found for the square planar Mo^{IV} and Os^{IV}, as well as for square pyramidal Os^{IV}, $Os^{IV}NCP^{\cdot\cdot}$ and Rh^{III}. Indeed, axial coordination is shown to increase the CShM in general, as this effect is larger with the cyanide ligand, but nothing else was obtained from that analysis. We also compared relevant BODSEP bond orders (bond orders normalized in such a way that their sum corresponds to the total number of bonds) to those reported in previous work by some of us.[27] These results can be found in SI Table S7. NCP-2H is said to be less aromatic than porphyrin. When one compares their dianion analogues, one can note that there is an increase in N-C_α bond order. If one assumes that the ideal aromatic value for these mixtures of single and double bonds is 1.5,[27] the anion of the NCP would seem to be more aromatic than that of porphyrin, which is contradictory. While metal coordination was shown to, on average, not influence this bond order, the same is not true in the case of NCP, as there is a slight decrease in the BODSEP of the N-C_α bond. The lateral M-N bond orders are comparable between the NCP complexes and those with porphyrin, but the M-C bond is exceptionally strong, thus weakening the opposite M-N bond, as can be noted by average bond order values close to 0.300. Unsurprisingly, the bond between the metal and the high-field ligand is stronger than that of the metal-chloride.

Electronic properties

The porphyrin absorption spectrum shows a triade of smaller intensity bands at higher wavelengths, the Q bands, and an absorption maximum at a higher energy wavelength, so called Soret band (B band). This spectrum has been tentatively interpreted with a four-orbital model originally proposed by Gouterman,[43] which states that these bands arise from π–π* transitions between the HOMO/HOMO-1 and the LUMO/LUMO+1 pairs, with varying degrees of bonding and antibonding character depending on substituents, and the effect of such ring substituents and metal coordination has been revisited by other computational chemists.[44,45]

We will thus be performing a similar analysis for the N-confused isomer and respective metalloNCPs. The comparison between the Soret band region of normal porphyrin, the NCP-2H isomer and the corresponding dianion, $NCP\text{-}2H^{2-}$, is in Figure 2. All the spectra presented in this section were calculated in DMF, as it is the solvent in which the confused porphyrin isomer was isolated.

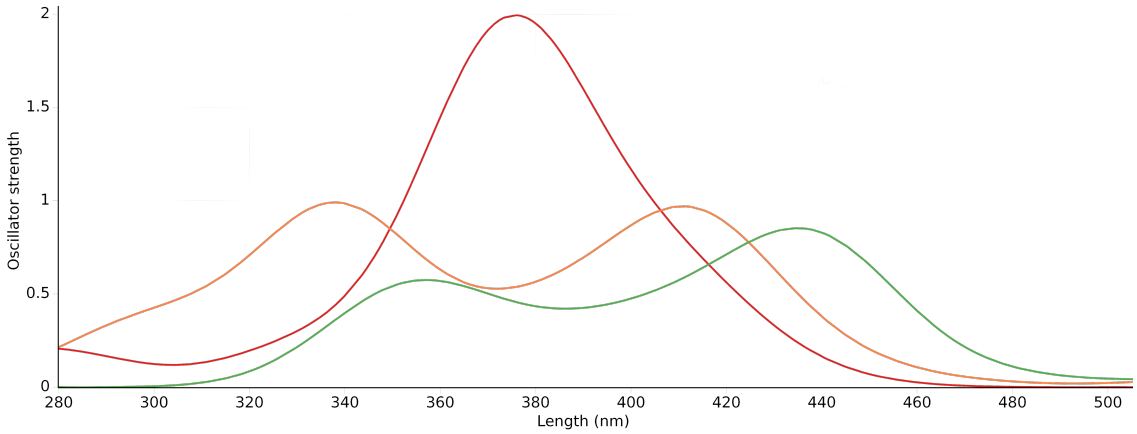

Fig. 2. Absorption spectra (dimethylformamide) calculated in the Soret band region of porphyrin (red) NCP-2H (orange) and its dianionic form (green). Band width = 40 nm, Gaussian height broadening.

The single band that was obtained for porphyrin around ca. 375 nm is in good agreement with the literature. This band appears to split into two bands with lower absorption values, in both NCP-2H and its dianionic form. However, if the average between the two absorption peaks is taken, porphyrin and its N-confused isomer have similar energies (porph ~375 nm, NCP-2H ~375 nm) and a small bathochromic shift is expected for the free base (free base ~400 nm). Scheme 7 provides a more in-depth investigation of the origin of these bands.

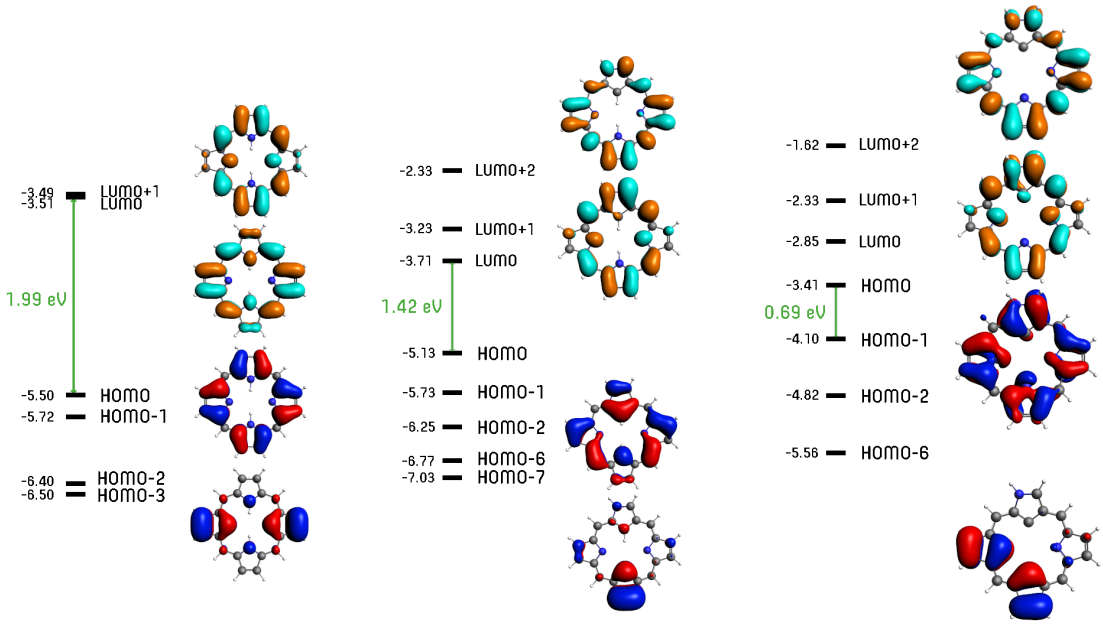

Scheme 7. Frontier orbital diagram for porphyrin (left), NCP-2H (center) and NCP-2H^{2-} (right). The orbitals involved in the Soret-band associated electronic transitions are depicted next to the corresponding diagram.

Despite the decrease in the HOMO-LUMO gap that is clearly noticeable from left to right in Sheme 7, what seems to contribute most to the differences in the calculated UV-Vis spectra is the decrease in the symmetry level of the N-confused monomer when compared to normal porphyrin. The orbitals involved in the electronic transitions of porphyrin are highly symmetric, cover most of the ring and agree with the four orbital model that states the orbitals involved in the transitions should be in the

frontier region (HOMO-3, HOMO-2). The same is not true, however, for the N-confused isomer. The decrease in ΔHOMO-LUMO explains the lowest energy band observed at ca. 410nm, but electron transitions accounting for a higher energy band (ca. 340 nm) are also noted. These electrons stem from orbitals that are much lower in energy (HOMO-7), in contradiction with the four-orbital model. A similar phenomenon is observed for the dianion.

No significant changes are observed between the UV-Vis spectrum of the dianion NCP-2H^{2-} and most of the transition metal complexes, except for the Rh complexes. These are shown in Figure 3 and that of the Os(II) complexes is shown in the SI as representative of the others (Figure S1).

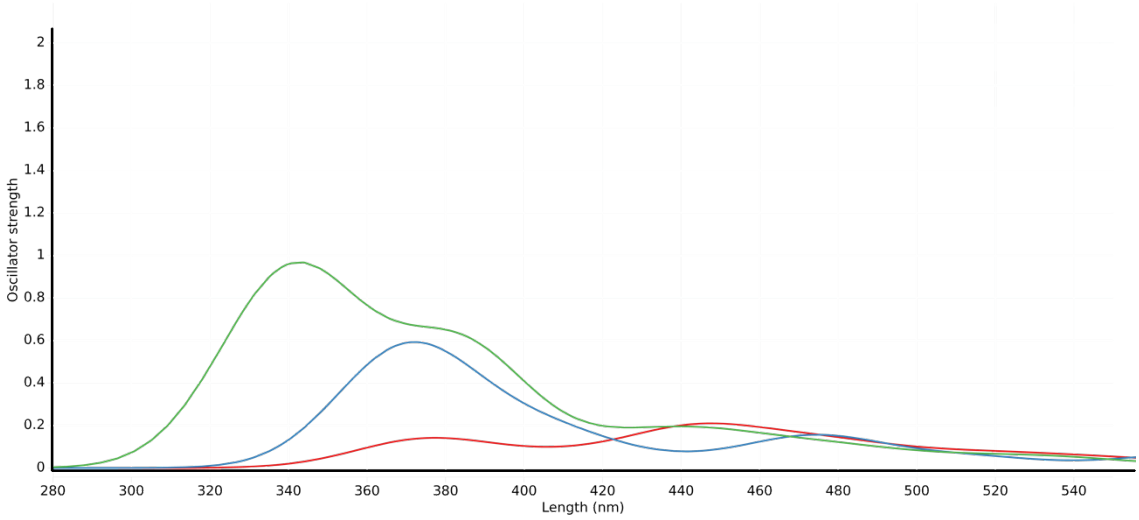

Fig. 3. UV-Vis spectra calculated in the Soret band region of (NCP)M (red), (NCP)M-Cl (blue) and (NCP)M-CN (green) for the Rh metal complexes. Band width = 40 nm, Gaussian height broadening.

The spectra in Figure 3 show a large ligand to metal charge transfer band that occur from π orbitals in the NCP ring to the d_{z2} metal orbital (Scheme S1 – Rh(NCP) HOMO/LUMO orbitals). The introduction of an axial ligand in the Rh(III) NCP not only increases the intensity of the band, but also its energy. This increase seems to be correlated with the strength of the field induced by the axial ligand which suggest it may be tuned.

Figure 4 contains the ΔHOMO-LUMO for the bare and substituted metalloNCPs.

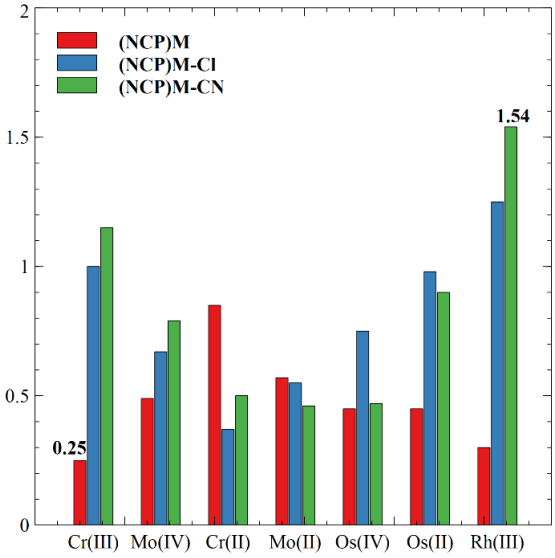

Fig. 4. HOMO-LUMO gaps for all the complexes in this work (energies in eV).

The HOMO-LUMO gap for NCP-2H is 1.42 eV as per Scheme 7. Analogous Zn and Mg complexes were reported to have HL gaps of (2.25 was obtained for the isomer NCP-2H) 2.21 eV and 2.14 eV.[46] The same result was obtained here, coordination to the transition-metal decreases this gap in all cases (Figure 4). However, as NCP-2H and its metal complexes do not exhibit the same Gouterman-type frontier orbitals, this parameter alone is not sufficient to explain their spectra. Most of the metal complexes have frontier orbitals that also have mostly a NCP ring character and π–π^* transitions occur, but that is not true for Os(II) or Rh(III), where both HOMO and LUMO are mostly located around the metal. In such cases the ligand π^* orbitals are in turn LUMO+2.

The two cases in which there is a massive increase in the gap from the normal to the Cl are Cr(III) and Rh(III). In both cases there is a massive destabilization of the LUMO orbital with respect to the HOMO (225% and 351% respectively) upon Cl coordination and this phenomenon is exacerbated further with the higher field ligand. The gap only decreases in Cr(II) and Mo(II). In both cases, the HOMO and LUMO orbitals for normal and the axial ligand analogues are very similar. They also have the same spin ground states for the bare NCP and Cl-coordinated (S=2 and S=1). Mo(II) has a smaller difference in H-L gap due to the largest destabilization of the LUMO orbital in regards to the HOMO in the Cl complex (143% vs 109%).

Redox chemistry of the rhodium-NCP radical

The $[Rh^{III}(NCP)]^+$ is best described as $[Rh^{IV}(NCP^{\cdot})]^+$ and it has been established that for Cr, Mo and Os a single oxidation state is accessible as the remaining redox chemistry occurs in the NCP ring. It is thus interesting to see what happens upon reduction and oxidation of the rhodium N-confused porphyrin as two oxidation states ($Rh^{III/IV}$) seem to be accessible. The reduction of $[Rh^{IV}NCP^{\cdot}]^+$ yields the neutral $[Rh^{II}NCP]$ doublet which is more stable than the quartet by ca. 27 kcal mol^{-1}. The oxidation of $[Rh^{IV}NCP^{\cdot}]^+$ yields a mixed configuration of quartet (more stable by ca. 0.04 kcal mol^{-1}) and doublet. The quartet corresponds to the oxidation of the metal to a FEC of $[Rh^{V}NCP^{\cdot}]^{2+}$ while the doublet is an oxidation of the NCP ligand, yielding the $[Rh^{IV}NCP]^{2+}$ species.

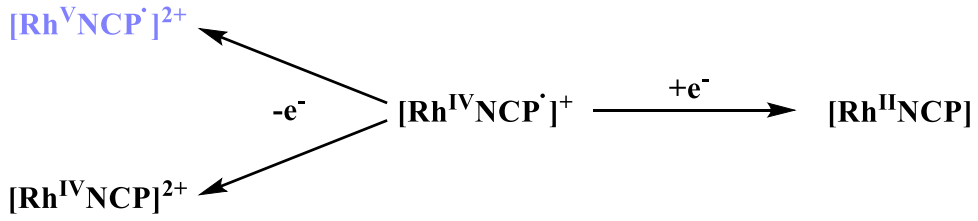

Scheme 8. Redox chemistry of the bare Rh N-confused porphyrin complex.

CONCLUSIONS

The electronic distribution and optical properties of the N-confused NCP-2H isomer and their transition metal complexes were analyzed. Our computational method proved to be successful in the description of both the geometries and spin states of known similar porphyrins. The spin state of the putative N-confused metalloporphyrins was shown to depend mostly on the total number of unpaired electrons and the same spin state was obtained for NCPs with seemingly equal number of *d* electrons, even with metals from different rows of the periodic table. An analysis of the electronic distribution in the bare metalloNCPs unveiled the redox character of the N-confused porphyrin. The introduction of an axial ligand was shown to affect the spin state of d^4 and d^5 complexes, as expected, but the effect is independent of the strength of the axial ligand field. Although in the porphyrin the electronic transitions associated to the B band region arise from frontier orbital excitations, the same is not true for NCP-2H or its metal complexes. This is problematic as the simple $\Delta_{HOMO-LUMO}$ gap analysis that is usually performed for the comparison of porphyrin derivatives is no longer possible for the N-confused analogues, the actual orbitals involved in the transitions must be studied as well. Here, the relative energy between the metal and ligand orbitals seems to be the determining factor: d^2, d^3, d^4 and Os(II) complexes showed a UV-Vis spectrum very similar to that of the dianion NCP-2H$^-$, while the d^5 Rh complexes showed a large LMCT band that is deeply affected by the axial destabilization of the metal *d* orbitals.

Computational details

DFT calculations were performed using the ADF/QUILD[47-49] program packages. Scalar relativistic corrections were employed using the Zeroth Order Regular Approximation[50] (ZORA). Solvent effects were included with the Conductor-like Screening Model (COSMO)[51] for dimethylformamide. Geometry optimizations, frequency, TD-DFT and single-point calculations were done with the S12g[28] functional and a triple-ζ basis set with double polarization functions[52] (S12g/TZ2P). Vibrational modes under 100 cm^{-1} were raised to this value when calculating Gibbs energies, to compensate for the breakdown of the harmonic oscillator model.[53-55]

Acknowledgements

The authors would like to thank AEI/MCIN (10.13039/501100011033) for funding (CTQ2017-87392-P, PID2020-114548GB-I00) and GenCat (2021 SGR 00487). FFM also thanks AEI/MCIN and the European Social Fund for a PhD studentship (PRE2018-083883).

REFERENCES

1. Bowman SEJ and Bren KL. *Natural Product Reports* 2008; **25**: 1118-1130.
2. Bonnett R. *Chemical Reviews* 1963; **63**: 573-605.
3. Pareek S, Sagar NA, Sharma S, Kumar V, Agarwal T, González-Aguilar GA and Yahia EM. *Fruit and Vegetable Phytochemicals* 2017; **29**: 269.
4. Drain CM, Varotto A and Radivojevic I. *Chemical Reviews* 2009; **109**: 1630-1658.
5. Pushpanandan P and Ravikanth M. *Topics in Current Chemistry* 2021; **379**: 26.
6. Chmielewski PJ, Latos-Grażyński L, Rachlewicz K and Glowiak T. *Angewandte Chemie International Edition* 1994; **33**: 779-781.
7. Furuta H, Asano T and Ogawa T. *Journal of the American Chemical Society* 1994; **116**: 767-768.
8. Furuta H, Ishizuka T, Osuka A, Dejima H, Nakagawa H and Ishikawa Y. *Journal of the American Chemical Society* 2001; **123**: 6207-6208.
9. Parr RG In *Horizons of Quantum Chemistry*; Fukui K, Pullman B, Eds.; Springer Netherlands: Dordrecht, 1980, pp 5-15.
10. Marchand G, Roy H, Mendive-Tapia D and Jacquemin D. *Physical Chemistry Chemical Physics* 2015; **17**: 5290-5297.
11. Tuersun M and Kerim A. *Royal Society Open Science*; **7**: 200069.
12. Furuta H, Maeda H and Osuka A. *The Journal of Organic Chemistry* 2001; **66**: 8563-8572.
13. Babu B, Mack J and Nyokong T. *New Journal of Chemistry* 2021; **45**: 5654-5658.
14. Wang L-L, Peng S-H, Wang H, Ji L-N and Liu H-Y. *Physical Chemistry Chemical Physics* 2018; **20**: 20141-20148.
15. Khodov IA, Maltceva OV, Klochkov VV, Koifman OI and Mamardashvili NZ. *New Journal of Chemistry* 2017; **41**: 7932-7937.
16. Fukuda M, Mori S, Furuta H and Shimizu S. *Chemistry – An Asian Journal* 2019; **14**: 1697-1702.
17. Miyazaki T, Fukuyama K, Mashita S, Deguchi Y, Yamamoto T, Ishida M, Mori S and Furuta H. *ChemPlusChem* 2019; **84**: 603-607.
18. Halder N, Dzhemileva LU, Ramazanov IR, D'Yakonov VA, Dzhemilev UM and Rath H. *ChemMedChem* 2020; **15**: 632-642.
19. dela Cruz J-aB and Hung C-H. *Catalysis Science & Technology* 2021; **11**: 2144-2154.
20. Ge Y, Cheng G, Xu N, Wang W and Ke H. *Catalysis Science & Technology* 2019; **9**: 4255-4261.
21. dela Cruz J-aB, Ruamps M, Arco S and Hung C-H. *Dalton Transactions* 2019; **48**: 7527-7531.
22. Grover N and Sankar M. *Chemistry – An Asian Journal* 2020; **15**: 2192-2197.
23. Babu B, Mack J and Nyokong T. *Dalton Transactions* 2020; **49**: 15180-15183.
24. Sripothongnak S, Ziegler CJ, Dahlby MR and Nemykin VN. *Inorganic Chemistry* 2011; **50**: 6902-6909.
25. Miyazaki T, Yamamoto T, Mashita S, Deguchi Y, Fukuyama K, Ishida M, Mori S and Furuta H. *European Journal of Inorganic Chemistry* 2018; **2018**: 203-207.
26. Yang C-H, Dzugan SJ and Goedken VL. *Journal of the Chemical Society, Chemical Communications* 1986: 1313-1315.
27. Swart M. *Theoretical Chemistry Accounts* 2020; **139**: 160.
28. Swart M. *Chemical Physics Letters* 2013; **580**: 166-171.
29. Liu J, Fan Y-Z, Li X, Wei Z, Xu Y-W, Zhang L and Su C-Y. *Applied Catalysis B: Environmental* 2018; **231**: 173-181.
30. Huang T, Wu X, Weare WW and Sommer RD. *European Journal of Inorganic Chemistry* 2014; **2014**: 5662-5674.
31. Smieja JA, Omberg KM, Busuego LN and Breneman GL. *Polyhedron* 1994; **13**: 339-343.
32. Blusch LK, Craigo KE, Martin-Diaconescu V, McQuarters AB, Bill E, Dechert S, DeBeer S, Lehnert N and Meyer F. *Journal of the American Chemical Society* 2013; **135**: 13892-13899.

33. Sit PHL, Car R, Cohen MH and Selloni A. *Inorganic Chemistry* 2011; **50**: 10259-10267.
34. Mehara J, Koovakattil Surendran A, van Wieringen T, Setia D, Foroutan-Nejad C, Straka M, Rulíšek L and Roithová J. *Chemistry – A European Journal* 2022; **28**: e202201794.
35. Day CS, Do CD, Odena C, Benet-Buchholz J, Xu L, Foroutan-Nejad C, Hopmann KH and Martin R. *Journal of the American Chemical Society* 2022; **144**: 13109-13117.
36. Rodríguez JI, Ayers PW, Götz AW and Castillo-Alvarado FL. *The Journal of Chemical Physics* 2009; **131**: 021101.
37. Kitaura K and Morokuma K. *International Journal of Quantum Chemistry* 1976; **10**: 325-340.
38. Kingsbury CJ and Senge MO. *Coordination Chemistry Reviews* 2021; **431**: 213760.
39. Alvarez S, Alemany P, Casanova D, Cirera J, Llunell M and Avnir D. *Coordination Chemistry Reviews* 2005; **249**: 1693-1708.
40. Casanova D, Cirera J, Llunell M, Alemany P, Avnir D and Alvarez S. *Journal of the American Chemical Society* 2004; **126**: 1755-1763.
41. Cirera J, Ruiz E and Alvarez S. *Chemistry – A European Journal* 2006; **12**: 3162-3167.
42. Alvarez S and Llunell M. *Journal of the Chemical Society, Dalton Transactions* 2000: 3288-3303.
43. Gouterman M. *Journal of Molecular Spectroscopy* 1961; **6**: 138-163.
44. Baerends EJ, Ricciardi G, Rosa A and van Gisbergen SJA. *Coordination Chemistry Reviews* 2002; **230**: 5-27.
45. Liao M-S and Scheiner S. *The Journal of Chemical Physics* 2002; **117**: 205-219.
46. Wang Q, Song M, Song X and Bu Y. *Physical Chemistry Chemical Physics* 2019; **21**: 17209-17220.
47. Swart M and Bickelhaupt FM. *J Comput Chem* 2008; **29**: 724-734.
48. In *SCM, Theoretical Chemistry, Vrije Universiteit, Amsterdam, The Netherlands*; 2019.3 ed.; SCM, Theoretical Chemistry, Vrije Universiteit, Amsterdam, The Netherlands; Vol. ADF 2019.3, pp SCM, Theoretical Chemistry, Vrije Universiteit, Amsterdam, The Netherlands.
49. te Velde G, Bickelhaupt FM, Baerends EJ, Fonseca Guerra C, van Gisbergen SJA, Snijders JG and Ziegler T. *Journal of Computational Chemistry* 2001; **22**: 931-967.
50. Lenthe Ev, Baerends EJ and Snijders JG. *The Journal of Chemical Physics* 1993; **99**: 4597-4610.
51. Pye CC and Ziegler T. *Theoretical Chemistry Accounts* 1999; **101**: 396-408.
52. Van Lenthe E and Baerends EJ. *Journal of Computational Chemistry* 2003; **24**: 1142-1156.
53. Swart M, Rösler E and Bickelhaupt FM. *European Journal of Inorganic Chemistry* 2007; **2007**: 3646-3654.
54. Ribeiro RF, Marenich AV, Cramer CJ and Truhlar DG. *The Journal of Physical Chemistry B* 2011; **115**: 14556-14562.
55. Averkiev BB and Truhlar DG. *Catalysis Science & Technology* 2011; **1**: 1526-1529.